Water Resources Research

RESEARCH ARTICLE
10.1029/2020WR027112

Nonstationary Frequency Analysis of Censored Data: A Case Study of the Floods in the Yangtze River From 1470 to 2017

Bin Xiong[1], Lihua Xiong[1], Shenglian Guo[1], Chong-Yu Xu[2], Jun Xia[1], Yixuan Zhong[1], and Han Yang[1]

[1]State Key Laboratory of Water Resources and Hydropower Engineering Science, Wuhan University, Wuhan, China, [2]Department of Geosciences, University of Oslo, Oslo, Norway

Key Points:

- The nonstationarity and insufficient length of data impact the accuracy of design flood estimation
- The stationary and nonstationary models considering data type are developed by a covariate method and the likelihood principle
- Temporal information expansion by censored data corrects the underestimation of probability for rare flood events in the original models

Correspondence to:
L. Xiong,
xionglh@whu.edu.cn

Citation:
Xiong, B., Xiong, L., Guo, S., Xu, C.-Y., Xia, J., Zhong, Y., & Yang, H. (2020). Nonstationary frequency analysis of censored data: A case study of the floods in the Yangtze River from 1470 to 2017. *Water Resources Research*, *56*, e2020WR027112. https://doi.org/10.1029/2020WR027112

Received 13 JAN 2020
Accepted 7 AUG 2020
Accepted article online 11 AUG 2020

Abstract Censored data (CD) of floods, that is, the combination of systematic data (SD) and historical data, can help improve the robustness of flood frequency analysis, due to its temporal information expansion. However, in nonstationary flood frequency analysis, the approach to utilize the CD has rarely been investigated. In this study, a covariate-based nonstationary flood frequency analysis framework based on various likelihood functions using the generalized extreme value (GEV) distribution was built to utilize the CD, with uncertainty considered. This framework was applied to the study of the annual maximum flood frequency of the Yichang gauging station 44 km downstream of the Three Gorges Dam over the period from 1470 to 2017. A summer precipitation anomaly and a reservoir index were used as covariates to explain the variation of the distribution parameters. The results show that for either the SD or CD, the nonstationary models are preferred to the stationary ones by the deviance information criterion, and these nonstationary models may prove to be practical in engineering application, due to the acceptable uncertainty range in flood quantiles derived from covariates. Compared to the stationary or nonstationary models based on the SD, the corresponding model based on the CD results in a higher posterior mean and a smaller posterior standard deviation for the shape parameter of the GEV distribution. It is concluded that the use of historical information under the nonstationary frequency analysis framework may be remarkable in reducing design flood uncertainty, especially for the very small exceedance probability at the tail.

1. Introduction

Accuracy of flood frequency estimates is vital for the hydrological design (e.g., the capacities of reservoir, levees, and spillways) and risk management (e.g., protection against economic losses in terms of maintenance of hydraulic structures). In frequency analysis, the magnitudes of flood events corresponding to a specific frequency of occurrence are given via the probability distributions fitted by the past observed data. However, there are inaccurate flood estimates in flood frequency analysis for many basins, resulting from two main sources: The first is the nonstationarity of flood data caused by the various potential climate-induced and human-induced changes in the hydrological regimes; the second is the limited length of flood data, resulting in insufficient accuracy of estimation for the tail behavior denominated by low-frequency large-impact events (Payrastre et al., 2011); for example, systematic (gauging) data of no more than 50 years are commonly required to estimate a 100-year flood (the flood with 100-year recurrence interval).

In terms of the first issue, the stationarity of hydrological series in the traditional frequency analysis has been widely questioned (e.g., Gilroy & McCuen, 2012; Jiang et al., 2015; Milly et al., 2008; Su & Chen, 2019; Villarini et al., 2009). Traditional frequency analysis generally assumes that hydrological series is stationary, which means "free of trends, shifts, or periodicity (cyclicity)" (Salas, 1993), or which indicates there is no change in the relevant environmental factors (e.g., climate and/or land use) (Yang et al., 2019). However, due to the integrated driving of human activity (e.g., reservoir construction and urban expansion) and climate change, there is the nonstationarity in the flooding regimes, which makes the flood frequency analysis more complicated (Toonen, 2015). While many researchers reported the human activities-induced flood nonstationarity (e.g., López & Francés, 2013; Wang et al., 2017; Xiong et al., 2019), some literature also recognized the climate-induced nonstationarity, especially during climatic anomalies such as the Little Ice Age

(e.g., Swierczynski et al., 2012; Toonen, 2015; Vallve & Martin-Vide, 1998). Some studies demonstrated the climate informed hydrological frequency analysis (e.g., Kwon et al., 2008; Liu et al., 2015). In general, there are two methods to deal with the nonstationarity in the flood frequency analysis: The first is characterizing the present situation through directly correcting (i.e., normalizing) the data from periods which differ from the current state of the flood regime (Toonen, 2015); the second is the covariate method where certain covariates are used to explain the variation in the probability distribution parameters (Jiang et al., 2019; Katz et al., 2002; López & Francés, 2013; Yan et al., 2017). In the second method, the generalized additive models for location, scale, and shape parameters (GAMLSS) (Rigby & Stasinopoulos, 2005), due to their flexibility, were normally used to assess nonstationary flood series (Du et al., 2015; Villarini et al., 2009). The GAMLSS framework can flexibly include climate or human activity covariates. In order to deal with the uncertainty in the model parameters, the Bayesian inference has been used for the nonstationary frequency analysis (Ouarda & El-Adlouni, 2011; Sun et al., 2015; Xiong et al., 2019). And the uncertainty of model parameter estimates can be conveniently obtained through the prior and posterior distributions.

In addition to the consideration of the nonstationarity, accurate design flood estimate also depends on sufficient length of the sample data of flood. However, the duration of systematic observation data of runoff or flood rarely exceeds 50 years in many basins. This can lead to a large statistical inference error, especially for the estimates of the tail behavior dominated by the rare events, because various studies have shown that there are periodicities of more than 100 years in Holocene flood records (e.g., Brázdil et al., 2011; Macklin & Lewin, 2008). Therefore, the expansion of hydrologic information (i.e., temporal, spatial, or causal information) was highlighted (e.g., Merz & Blöschl, 2008a, 2008b; Viglione et al., 2013). These information expansions are generally considered to be able to reduce the uncertainty of flood estimates. In the literature, historical data, as a type of temporal information, have been combined with the systematic data (SD) to constitute the so-called censored data (CD) in flood frequency analysis (e.g., Bayliss & Reed, 2001; Kjeldsen et al., 2014; Li et al., 2013; Schendel & Thongwichian, 2017; Stedinger & Cohn, 1986). To deal with the CD in flood frequency analysis, a number of methods, such as the Bayesian method, the maximum likelihood, the expected moments algorithm, the historically weighted moments, the probability weighted moments, and the L-moments, have been proposed (England et al., 2019; Guo & Cunnane, 1991; Li et al., 2013; Wang, 1996). Among these methods, the Bayesian method was highlighted (Parkes & Demeritt, 2016; Reis & Stedinger, 2005; Steinschneider & Lall, 2015). Viglione et al. (2013) combined local flood data with the three types of information (i.e., temporal information, spatial information, and causal information) using Bayesian analysis and assessed the sensitivity of the final flood estimate to the assumption involved. However, these studies were applied under the stationary assumption. Recently, Machado et al. (2015) presented nonstationary modeling of flood frequency considering the historical data using the GAMLSS. However, their modeling method of separating the flood series into three segments, which greatly increases the model freedom, leads to the independent model parameters over different periods. Moreover, the uncertainty in the historical data and the uncertainty of model parameters were not taken into consideration.

Based on the above literature review, it is found that both the nonstationarity and the data length will have impacts on the accuracy of design flood estimates in flood frequency analysis. Therefore, how to comprehensively utilize the CD (i.e., the combination of the systematic and historical data) under the framework of the nonstationary flood frequency analysis needs to be carefully investigated.

The goal of this study is to incorporate the approach of expanding temporal information based on the CD into the nonstationary flood frequency analysis, as well as considering both the historical data uncertainty and the model parameter uncertainty. The organization of the paper is as follows. In section 2, the framework of covariate-based nonstationary flood frequency analysis of CD based on the generalized extreme value (GEV) distribution is presented. Section 3 describes the case study in the upper Yangtze River basin. Section 4 presents the conclusions and discussion.

2. Methods

The framework (Figure 1) of covariate-based nonstationary flood frequency analysis of CD is outlined as follows. First, the GEV distribution and covariate method to develop the stationary GEV (SGEV) and nonstationary GEV (NGEV) models were introduced. Second, under the stationary condition, depending on the

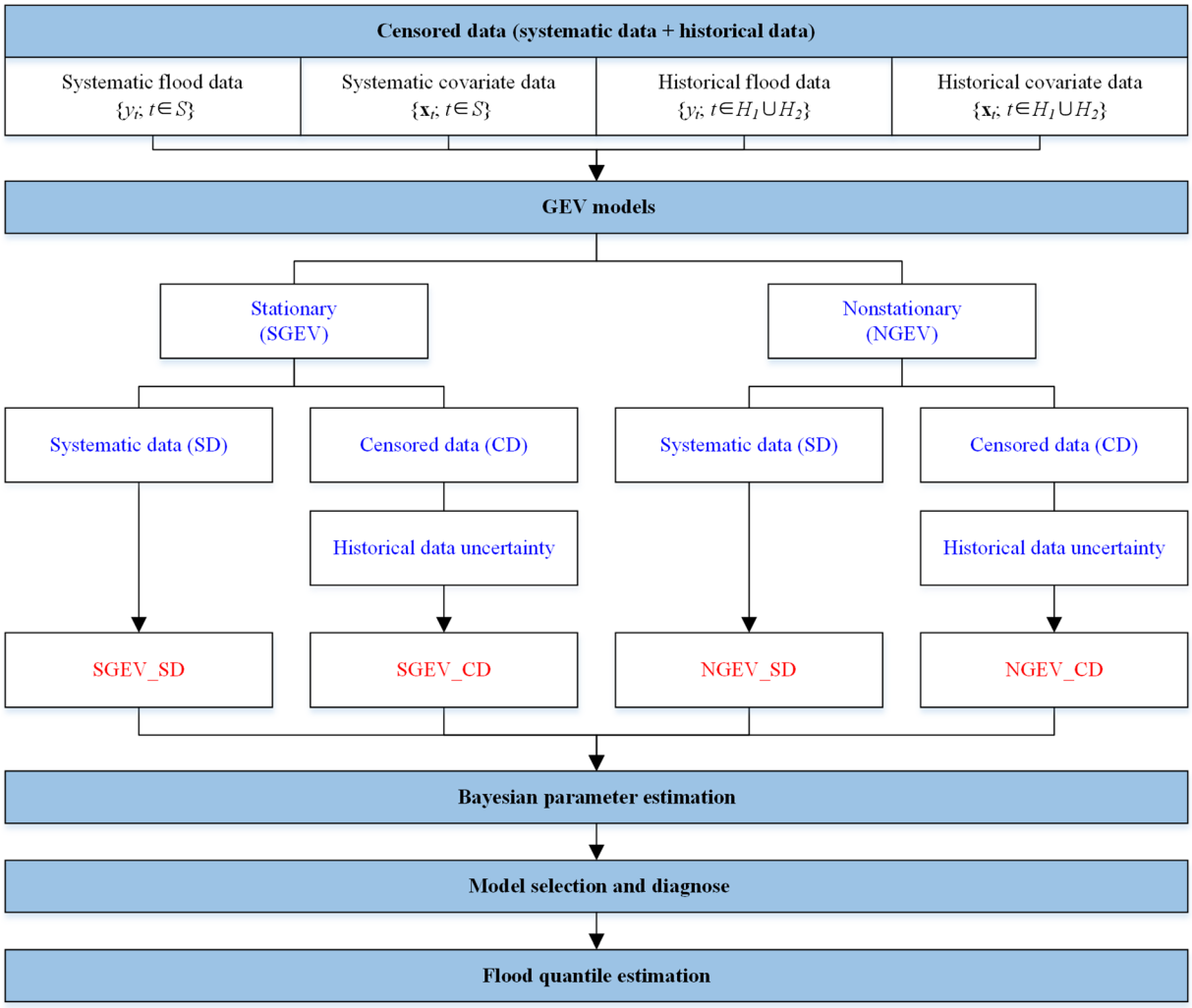

Figure 1. Flowchart of covariate-based nonstationary frequency analysis of censored data.

data type (either SD or CD), two SGEV models (i.e., SGEV_SD and SGEV_CD) were developed. Third, under the nonstationary condition, depending on the data type (either SD or CD), two NGEV models (i.e., NGEV_SD and NGEV_CD) were developed. Fourth, the Bayesian parameter estimation method was used to deliberate on the model parameter uncertainty. Finally, the methods of model selection and diagnosis were presented.

2.1. GEV Distribution

According to the Fisher-Tippett theorem, block maxima (a block being defined as a fixed time period such as a year) should follow the GEV distribution, a family of continuous probability distributions. The GEV distribution has been widely used to handle hydro-meteorological extreme events (e.g., De Paola et al., 2018; El Adlouni et al., 2007; Li et al., 2013; Martins & Stedinger, 2000; Ouarda & El-Adlouni, 2011; Viglione et al., 2013). Let flood variable Y_t follow the GEV distribution with a density function $f_{Y_t}(\cdot)$, which is given by

$$f_{Y_t}(y_t;\mu_t,\sigma_t,\xi_t) = \frac{1}{\sigma_t}\left[1+\xi_t\left(\frac{y_t-\mu_t}{\sigma_t}\right)\right]^{-\frac{1}{\xi_t}-1}\exp\left\{-\left[1+\xi_t\left(\frac{y_t-\mu_t}{\sigma_t}\right)\right]^{-\frac{1}{\xi_t}}\right\},$$
$$-\infty<\mu_t<\infty,\ \sigma_t>0,\ -\infty<\xi_t<\infty,\ 1+\xi_t\left(\frac{y_t-\mu_t}{\sigma_t}\right)>0, \quad (1)$$

where y_t is a realization of Y_t, μ_t is the location parameter, σ_t is the scale parameter, and ξ_t is the shape parameter.

2.2. Covariate Method

In the covariate-based nonstationary frequency analysis, the distribution parameters are assumed to be dependent on certain covariates. For the GEV distribution, it is commonly assumed that the distribution parameters μ_t and/or σ_t are dependent on covariates whereas ξ_t is always constant, because ξ_t is quite sensitive and tough to be estimated (Du et al., 2015; Xiong et al., 2019). A vector of covariates (of length n) $\mathbf{X}_t = [X_{1t}, X_{2t}, ..., X_{nt}]$ to explain the nonstationarity of flood series can be incorporated by the generalized linear additive formulation based on the GAMLSS (Rigby & Stasinopoulos, 2005; Stasinopoulos & Rigby, 2007). The global model is adopted in this paper; that is, all covariates are considered to explain each of distribution parameters μ_t and σ_t, which is expressed as follows:

$$\begin{aligned} g_1(\mu_t) &= \alpha_0 + \alpha_1 X_{1t} + ... + \alpha_n X_{nt}, \\ g_2(\sigma_t) &= \beta_0 + \beta_1 X_{1t} + ... + \beta_n X_{nt}, \\ \xi_t &= \xi, \end{aligned} \tag{2}$$

where both $\boldsymbol{\alpha} = [\alpha_0, \alpha_1, ..., \alpha_n]$ and $\boldsymbol{\beta} = [\beta_0, \beta_1, ..., \beta_n]$ are the model parameters to be estimated; the vector of all the model parameters in Equation 2 is denoted by $\boldsymbol{\theta} = [\boldsymbol{\alpha}, \boldsymbol{\beta}, \xi]$; $g_1(\cdot)$ and $g_2(\cdot)$ are the link functions. In this study, $g_2(\cdot)$ is assumed to be the logarithmic function to give a positive scale, while $g_1(\cdot)$ is assumed to be the identity or the logarithmic function by following the previous studies (Jiang et al., 2019; Read & Vogel, 2016; Sarhadi et al., 2016) to capture potential linear or nonlinear dependence of μ_t on the covariates $\mathbf{X}_t$. Thus, the candidate formulas for calculating μ_t in the global model are given by

$$\begin{aligned} &\text{Linear:} && \mu_t = \alpha_0 + \alpha_1 X_{1t} + ... + \alpha_n X_{nt}. \\ &\text{Exponential:} && \mu_t = \exp(\alpha_0 + \alpha_1 X_{1t} + ... + \alpha_n X_{nt}). \end{aligned} \tag{3}$$

2.3. SGEV Models

In the stationary condition, no covariate will be incorporated. According to Equation 2, the stationary models have only three model parameters, that is, $\boldsymbol{\theta} = [\alpha_0, \beta_0, \xi]$.

2.3.1. SGEV_SD Model

SD are data where values are systematically recorded by the gauging station. Based on the joint probability of occurrence of the SD, the log likelihood function in the stationary condition is given by

$$l_{\text{SGEV\_SD}}(\boldsymbol{\theta}) = \sum_{t \in S} \ln f_{Y_t}(y_t; \boldsymbol{\theta}), \tag{4}$$

where l is log likelihood, SGEV_SD is the model code of the SGEV distribution based on the SD, and S is the set of the years corresponding to the systematic floods.

2.3.2. SGEV_CD Model

CD are the combination of both SD and historical data. In this study, the historical data are divided into two groups, one with known values and the other with unknown values. Those historical floods whose values have been predetermined or estimated by some methods are called known historical floods, while the remaining historical floods are called unknown historical floods, whose values are all assumed to be below a given threshold. Based on the joint probability of occurrence of the CD, the log likelihood function in the stationary condition is given by

$$l_{\text{SGEV\_CD}}(\boldsymbol{\theta}) = \sum_{t \in S} \ln f_{Y_t}(y_t; \boldsymbol{\theta}) + \sum_{t \in H_1} \ln\left(f_{Y_t}(y_t; \boldsymbol{\theta})\right) + \sum_{t \in H_2} \ln(F_{Y_t}(z; \boldsymbol{\theta})), \tag{5}$$

where SGEV_CD is the model code of the SGEV distribution based on the CD, H_1 is the set of the years corresponding to the known historical floods, H_2 is the set of the years corresponding to the unknown historical floods whose values are below the assumed threshold z, and $F_{Y_t}(\cdot)$ is the cumulative distribution function of Y_t.

To consider the uncertainty in both determining the magnitudes of the known historical floods and assuming a threshold value to characterize the unknown historical floods, it is assumed that random errors associated with y_t ($t \in H_1$) and z, denoted by E_{y_t} and E_z, respectively, are normally distributed with zero means and constant standard deviations. The probability density functions for E_{y_t} and E_z are written as

$$\begin{aligned} f_{E_{y_t}}(\varepsilon_{y_t}) &= N(\varepsilon_{y_t}; 0, \delta_y), \\ f_{E_z}(\varepsilon_z) &= N(\varepsilon_z; 0, \delta_z), \end{aligned} \tag{6}$$

where ε_{y_t} and ε_z are the realizations of random error variables E_{y_t} and E_z, respectively, with δ_y and δ_z being the corresponding standard deviations of E_{y_t} and E_z. The log likelihood function conditional on $\boldsymbol{\delta} = [\delta_y, \delta_z]$ is given by

$$\begin{aligned} l_{\text{SGEV\_CD}}(\boldsymbol{\theta}|\delta_y, \delta_z) = &\sum_{t \in S} \ln f_{Y_t}(y_t; \boldsymbol{\theta}) + \sum_{t \in H_1} \left[\int_{\Omega_{\varepsilon_y}} \left(\ln f_{Y_t}(y_t + \varepsilon_{y_t}; \boldsymbol{\theta}) \right) \cdot f_{E_{y_t}} d\varepsilon_{y_t} \right] \\ &+ \sum_{t \in H_2} \left[\int_{\Omega_{\varepsilon_z}} \left(\ln F_{Y_t}(z + \varepsilon_z; \boldsymbol{\theta}) \right) \cdot f_{E_z} d\varepsilon_z \right], \end{aligned} \tag{7}$$

where Ω_{ε_y} and Ω_{ε_z} are the domains of ε_{y_t} and ε_z, respectively. It is almost impossible to get analytical integration for the integrals in Equation 7. Let $\left\{ \varepsilon_{y_t}^1, \ldots, \varepsilon_{y_t}^{\widetilde{n}}, \varepsilon_z^1, \ldots, \varepsilon_z^{\widetilde{n}} \right\}$ be an independent sample from the error distributions $f_{E_{y_t}}$ and f_{E_z}, where $\widetilde{n}$ is the sample size. In the model parameter computation, these integrals are approximated by

$$\begin{aligned} &\int_{\Omega_{\varepsilon_y}} \left(\ln f_{Y_t}(y_t + \varepsilon_{y_t}; \boldsymbol{\theta}) \right) \cdot f_{E_{y_t}} d\varepsilon_{y_t} \approx \frac{1}{\widetilde{n}} \sum_{k=1}^{\widetilde{n}} \left(\ln f_{Y_t}\left(y_t + \varepsilon_{y_t}^k; \boldsymbol{\theta} \right) \right), \\ &\int_{\Omega_{\varepsilon_z}} \left(\ln F_{Y_t}(z + \varepsilon_z; \boldsymbol{\theta}) \right) \cdot f_{E_z} d\varepsilon_z \approx \frac{1}{\widetilde{n}} \sum_{k=1}^{\widetilde{n}} \left(\ln F_{Y_t}(z + \varepsilon_z^k; \boldsymbol{\theta}) \right). \end{aligned} \tag{8}$$

2.4. NGEV Models

In the nonstationary condition, certain covariates will be incorporated to explain the variation of the distribution parameters. The nonstationary models have more than three parameters, that is, $\boldsymbol{\theta} = [\boldsymbol{\alpha}, \boldsymbol{\beta}, \xi]$. Technically, according to Equation 2, different vector $\mathbf{x}_t$ as the realizations of $\mathbf{X}_t$ will give different location and scale parameters which generate different probability density distributions for flood variable Y_t, but all these location and scale parameters are calculated from the same parameter vector $\boldsymbol{\theta}$. For a single sample $(y_t, \mathbf{x}_t)$, the conditional density function is notated as $f_{Y_t}(y_t|\mathbf{x}_t; \boldsymbol{\theta})$ and the conditional cumulative distribution function is notated as $F_{Y_t}(y_t|\mathbf{x}_t; \boldsymbol{\theta})$. It should be noted that Equation 2 is just one of the many possible formulas that can be used in deriving the distribution parameters from the related covariates. The final formulas for calculating μ_t and σ_t can be determined by the covariate selection analysis.

2.4.1. NGEV_SD Models

Based on the joint probability of occurrence of the SD, the log likelihood function in the nonstationary condition is given by

$$l_{\text{NGEV\_SD}}(\boldsymbol{\theta}) = \sum_{t \in S} \ln f_{Y_t}(y_t|\mathbf{x}_t; \boldsymbol{\theta}), \tag{9}$$

where NGEV_SD is the model code of the NGEV distribution based on the SD.

2.4.2. NGEV_CD Models

Based on the joint probability of occurrence of the CD, the log likelihood function in the nonstationary condition is given by

$$l_{\mathrm{NGEV\_CD}}(\theta) = \sum_{t \in S} \ln f_{Y_t}(y_t|\mathbf{x}_t;\theta) + \sum_{t \in H_1} \ln f_{Y_t}(y_t|\mathbf{x}_t;\theta) + \sum_{t \in H_2} \ln F_{Y_t}(z|\mathbf{x}_t;\theta), \tag{10}$$

where NGEV_CD is the model code of the NGEV distribution based on the CD.

For the nonstationary model based on the CD, in addition to the uncertainty in the historical flood data, the uncertainty in the historical covariate data $\mathbf{x}_t$ is considered. It is also assumed that random errors associated with each value of X_{it} ($i = 1,2,...,n$), which are denoted by $E_{x_{it}}$, are normally distributed with zero means and constant standard deviations. The probability density functions of $E_{x_{it}}$ are written as

$$f_{E_{x_{it}}}(\varepsilon_{x_{it}}) = N(\varepsilon_{x_{it}};0,\delta_{x_i}),\ i = 1,\ 2,\ ...,\ n, \tag{11}$$

where $\varepsilon_{x_{it}}$ is the realization of $E_{x_{it}}$ with δ_{x_i} being the corresponding standard deviation of $E_{x_{it}}$.

Take one covariate as an example. In the nonstationary condition, the log likelihood function conditional on standard deviation $\boldsymbol{\delta} = [\delta_y, \delta_z, \delta_{x_1}]$ is given by

$$\begin{aligned} l_{\mathrm{NGEV\_CD}}(\theta|\delta_y,\delta_z,\delta_{x_1}) &= \sum_{t \in S} \ln f_{Y_t}(y_t|x_{1t};\theta) \\ &+ \sum_{t \in H_1} \left[\iint_{\Omega_{\varepsilon_y,\,\varepsilon_{x_1}}} \left(\ln f_{Y_t}(y_t + \varepsilon_{y_t}|x_{1t} + \varepsilon_{x_{1t}};\theta)\right) \cdot f_{E_{y_t}} \cdot f_{E_{x_{1t}}} d\varepsilon_{y_t} d\varepsilon_{x_{1t}} \right] \\ &+ \sum_{t \in H_2} \left[\iint_{\Omega_{\varepsilon_z,\,\varepsilon_{x_1}}} \left(\ln F_{Y_t}(z + \varepsilon_z|x_{1t} + \varepsilon_{x_{1t}};\theta)\right) \cdot f_{E_z} \cdot f_{E_{x_{1t}}} d\varepsilon_z d\varepsilon_{x_{1t}} \right], \end{aligned} \tag{12}$$

where $\Omega_{\varepsilon_y,\,\varepsilon_{x_1}}$ and $\Omega_{\varepsilon_z,\,\varepsilon_{x_1}}$ are the two-dimensional domains of errors. There are also no analytical integrations for the double integrals in Equation 12. Let $\left\{\varepsilon_{y_t}^1, ..., \widetilde{\varepsilon_{y_t}^n}, \varepsilon_{x_{1t}}^1, ..., \widetilde{\varepsilon_{x_{1t}}^n}, \varepsilon_z^1, ..., \widetilde{\varepsilon_z^n}\right\}$ be an independent sample from the error distributions $f_{E_{y_t}}$, f_{E_z}, and $f_{E_{x_{1t}}}$. In the model parameter computation, these integrals are approximated by

$$\begin{aligned} &\iint_{\Omega_{\varepsilon_y,\,\varepsilon_{x_1}}} \left(\ln f_{Y_t}(y_t + \varepsilon_{y_t}|x_{1t} + \varepsilon_{x_{1t}};\theta)\right) \cdot f_{E_{y_t}} \cdot f_{E_{x_{1t}}} d\varepsilon_{y_t} d\varepsilon_{x_{1t}} \approx \\ &\qquad \frac{1}{\widetilde{n}} \sum_{k=1}^{\widetilde{n}} \left(\ln f_{Y_t}\left(y_t + \varepsilon_{y_t}^k|x_{1t} + \varepsilon_{x_{1t}}^k;\theta\right)\right), \\ &\iint_{\Omega_{\varepsilon_z,\,\varepsilon_{x_1}}} \left(\ln F_{Y_t}(z + \varepsilon_z|x_{1t} + \varepsilon_{x_{1t}};\theta)\right) \cdot f_{E_z} \cdot f_{E_{x_{1t}}} d\varepsilon_z d\varepsilon_{x_{1t}} \approx \\ &\qquad \frac{1}{\widetilde{n}} \sum_{k=1}^{\widetilde{n}} \left(\ln F_{Y_t}\left(z + \varepsilon_z^k|x_{1t} + \varepsilon_{x_{1t}}^k;\theta\right)\right). \end{aligned} \tag{13}$$

2.5. Bayesian Parameter Estimation

The vector of model parameters to be estimated for the models (SGEV_SD, SGEV_CD, NGEV_SD, and NGEV_CD) is uniformly expressed as $\theta = [\alpha, \beta, \xi]$. The Bayesian inference method (Ouarda & El-Adlouni, 2011; Xiong et al., 2019) is used to estimate θ. According to the Bayes' theorem, the posterior probability distribution $p(\theta|\mathrm{AD})$ can be expressed as

$$p(\theta|\mathrm{AD}) = \frac{L(\mathrm{AD}|\theta)\pi(\theta)}{\int_\Phi L(\mathrm{AD}|\theta)\pi(\theta)d\theta} \propto L(\mathrm{AD}|\theta)\pi(\theta), \tag{14}$$

where AD represents the available data (either SD or CD), $\pi(\cdot)$ is the prior probability distribution function, $L(\cdot)$ is the likelihood function, the integral $\int_\Phi$ is the normalizing constant, and Φ is the entire parameter space. The posterior distributions of model parameters in Equation 14 can be calculated through the Markov chain Monte Carlo (MCMC) methods (El Adlouni et al., 2007; Laloy & Vrugt, 2012; Martins & Stedinger, 2000; Vrugt et al., 2009).

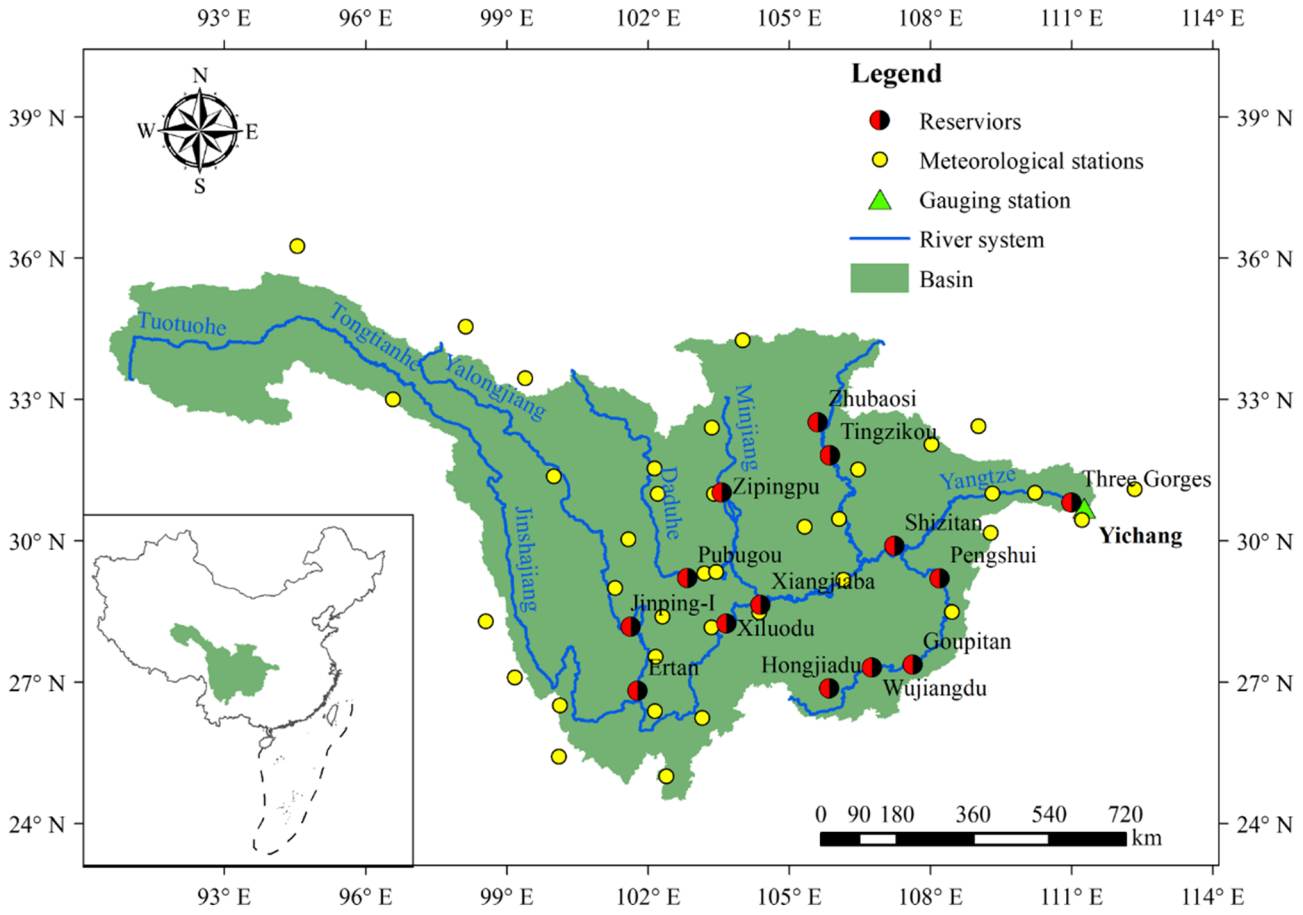

Figure 2. Location, topography, and river systems in the upper Yangtze River basin.

2.6. Model Selection and Diagnosis

In this study, same covariates are added to NGEV_SD and NGEV_CD models. And covariate selection analysis of NGEV_SD models is carried out. In the Bayesian framework, covariate selection is based on the posterior distribution of the deviance $D = -2l\left(\mathrm{AD}\middle|\hat{\theta}\right)$. A simple way to compare two models is through the deviance information criterion (DIC; Spiegelhalter et al., 2002, 2014):

$$\mathrm{DIC} = \overline{D} + p_D, \tag{15}$$

where $\overline{D}$ measuring the goodness of fit of model to the data is the posterior mean of D; p_D measuring the effective number of parameters is equal to $\overline{D} - \widehat{D}$, where $\widehat{D}$ denotes the deviance at the parameter posterior mean. The fitted NGEV_SD object with a lower DIC value will be preferred. The optimal NGEV_SD and NGEV_CD models in the covariate selection are denoted as $^{\mathrm{opt}}$NGEV_SD and $^{\mathrm{opt}}$NGEV_CD, respectively.

The models (SGEV_SD, SGEV_CD, $^{\mathrm{opt}}$NGEV_SD, and $^{\mathrm{opt}}$NGEV_CD) are evaluated further by checking the goodness of fit and the uncertainty in quantile estimation. In testing the goodness of fit, the quantile-quantile plot based on the diagnosis method (Coles, 2001) is used. A good model should have the plotted points close to the 1:1 line.

3. Case Study

3.1. Upper Yangtze River Basin

The upper Yangtze River basin with the area of 1×10^6 km^2 is selected as an illustrative case. Location, topography, and river systems in the upper Yangtze River basin are presented in Figure 2. The mean annual flow

Table 1
Information on the Reservoirs in the Upper Yangtze River Basin

Number	Name	Completion year	Total capacity (10^9 m^3)	River	Longitude	Latitude
1	Shizitan	1956	1.02	Longxihe	29.89	107.24
2	Wujiangdu	1983	2.30	Wujiang	27.32	106.76
3	Ertan	1998	6.14	Yalongjiang	26.82	101.78
4	Zhubaosi	1998	2.55	Jialingjiang	32.52	105.61
5	Zipingpu	2006	1.11	Minjiang	31.03	103.57
6	Hongjiadu	2006	4.95	Wujiang	26.87	105.85
7	Pubugou	2008	5.33	Daduhe	29.21	102.84
8	Pengshui	2009	1.47	Wujiang	29.20	108.20
9	Three Gorges	2009	39.30	Yangtze	30.82	111.00
10	Goupitan	2011	5.56	Wujiang	27.37	107.63
11	Xiangjiaba	2013	5.16	Jinshajiang	28.64	104.40
12	Xiluodu	2014	12.67	Jinshajiang	28.24	103.67
13	Jinping-I	2014	7.76	Yalongjiang	28.18	101.64
14	Tingzikou	2014	4.07	Jialingjiang	31.82	105.87

and runoff volume (1882–2017) of Yichang gauging station 44 km downstream of Three Gorges Dam are 14,068 m^3/s and 443.9 × 10^9 m^3, respectively. The average annual precipitation of the whole area is 1,033.2 mm. Since 1998, in the upper Yangtze River basin, many large reservoirs have been constructed, the location of which is shown in Figure 2. The hydrological regime in this area has been significantly affected by the operation of these reservoirs. After the Three Gorges Reservoir with the world's largest power station became fully operational in 2009, the downstream hydrological regime experienced a greater reservoir-induced change than that in the past (Gao et al., 2013).

3.2. Covariates

3.2.1. Summer Precipitation Anomaly

In the case study, summer (May–September) precipitation anomaly (SPA), as a covariate, is incorporated to consider the effects of climate on flood variations. The SPA is defined as the departure of summer mean precipitation from its long-period average value, the unit of which is mm/day. To obtain the annual series of the SPA in the basin area from 1470 to 2017, the precipitation reconstruction data set (1470–2000) of Shi et al. (2017) and the precipitation gauge data (1951–2017) of the National Climate Center of the China Meteorological Administration, China, were used in this study. The climate reconstruction data set,

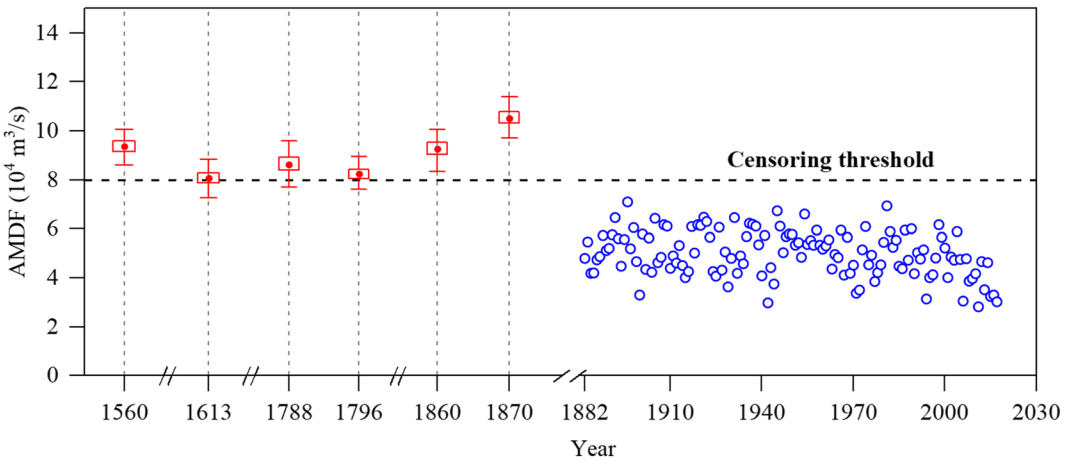

Figure 3. Time series of annual maximum daily flood (AMDF) in the upper Yangtze River basin. The known historical floods whose uncertainty is equal to the 30% standard deviation of AMDF samples are indicated by the red symbols. The vertical dashed lines are the grid lines at the years of these known historical floods along the axis. Systematic floods are indicated by the blue points.

Table 2
A List of the Known Historical Floods Whose Annual Maximum Daily Flood (AMDF) Is Over 80,000 m^3/s Since 1470 and the Corresponding Values of the Summer Precipitation Anomaly (SPA) and the Reservoir Index (RI) in the Upper Yangtze River Basin

Year	AMDF (m^3/s)	SPA (mm/day)	RI (-)
1560	93,600	0.12	0.00
1613	81,000	0.57	0.00
1788	86,000	0.63	0.00
1796	82,200	−0.14	0.00
1860	92,500	0.28	0.00
1870	105,000	0.42	0.00

consisting of multiproxy May–September average precipitation field (mm/day) reconstructions with spatial resolution 0.5° × 0.5° for China, has been cited by many pieces of research (e.g., Brázdil et al., 2018; Hua et al., 2019). This data set is based on 372 tree-ring chronologies and 107 historical documentary records and had been validated by two instrumental precipitation data sets, that is, the China Ground Precipitation 0.5° × 0.5° Grid Dataset V2.0 (Zhao & Zhu, 2015), a monthly gridded precipitation data set, covering the period 1961–2010, and the Homogenized Monthly Precipitation Dataset in China, covering the interval 1900–2009 (Li et al., 2012), with a 5 longitude by 5 latitude grid resolution. Considering the uncertainty of the SPA reconstruction in the historical period, uncertainty scenarios are designed and illustrated in section 3.4.

3.2.2. Reservoir Index

Another covariate, the reservoir index (RI) is employed to consider the effects of reservoirs on flood variations. According to the previous studies (Batalla et al., 2004; Li et al., 2015; López & Francés, 2013; Lu et al., 2020; Wang et al., 2017; Xiong et al., 2019), there are different formulas to define the RI. For clarity, the RI for a gauge station is defined as

$$\mathrm{RI} = \frac{\sum_{i=1}^{M} C_i}{R_m}, \tag{16}$$

where M is the total number of reservoirs upstream of the gauging station, C_i is the maximum storage capacity of reservoir i upstream of the gauge station, and R_m is the multiyear mean runoff at the gauge station. Thus, the RI is the ratio of the total storage capacity of all reservoirs upstream of the gauge station to the multiyear mean runoff, representing the degree of reservoir effects. In this study, considering that it is difficult to collect the detailed information of reservoir operations and inflows for calculating a more complex index in the upper Yangtze River basin, the simple RI as shown in Equation 16 is used. Another consideration for the RI selection is that it would be difficult to determine whether a complex or simple index is more efficient, because the length of the flood samples affected by the reservoirs is short. The information of the reservoirs in the upper Yangtze River basin was collected to calculate the RI. Table 1 summarizes the information of the reservoirs of which the capacity is more than 1×10^9 m^3 in the case area.

3.3. Flood Data

In this section, censored flood samples arising in annual maximum daily flood (AMDF) of the Yichang gauging station were elucidated. According to Li et al. (2013), since the last century, the Changjiang Water Resources Commission (CWRC) has investigated a lot of historical flood events in the study area. In order to take a reliable design of the Three Gorges Project, the gathered historical information was quantificationally summarized as the eight largest historical floods since 1153 by CWRC and other relevant units (CWRC, 1996) and all the unknown floods in the historical period (1153–1881) have been determined to be below a fixed censoring threshold (CT) of 80,000 m^3/s as shown in Figure 3 (Li et al., 2013), that is, z = CT =80,000 m^3/s, where z is the threshold value involved in the CD and defined in Equation 5.

In this study, the study period was set as 1470 to 2017, considering the limitation of covariate data length. Thus, the censored flood data consist of systematic flood data and historical flood data (Figure 3). The systematic flood data include the observations of 136 years (1882–2017), which is extracted from the systematic daily flow data

Table 3
Six Uncertainty Scenarios Defined in Terms of the Standard Deviation δ of the Random Error ε Associated With the Annual Maximum Daily Flood (AMDF) of the Six Known Historical Floods, the Censoring Threshold (CT) Characterizing the Unknown Historical Floods, and the Summer Precipitation Anomaly (SPA) During the Historical Period (1470–1881)

Scenario codes	Standard deviation of random errors		
	$\delta_{\varepsilon_{AMDF}}$ (m^3/s)	$\delta_{\varepsilon_{CT}}$ (m^3/s)	$\delta_{\varepsilon_{SPA}}$ (mm/day)
S0	0.0 (0% δ_{AMDF})	0	0.00 (0% δ_{SPA})
S1	0.0 (0% δ_{AMDF})	8,000	0.00 (0% δ_{SPA})
S2	1,227.0 (10% δ_{AMDF})	0	0.030 (10% δ_{SPA})
S3[a]	1,227.0 (10% δ_{AMDF})	8,000	0.030 (10% δ_{SPA})
S4	3,681.1 (30% δ_{AMDF})	8,000	0.089 (30% δ_{SPA})
S5	6,135.2 (50% δ_{AMDF})	8,000	0.148 (50% δ_{SPA})

Note. δ_{AMDF} and δ_{SPA} are the standard deviations of AMDF samples and SPA samples in the study area, respectively.
[a]Representative scenario for the model comparison.

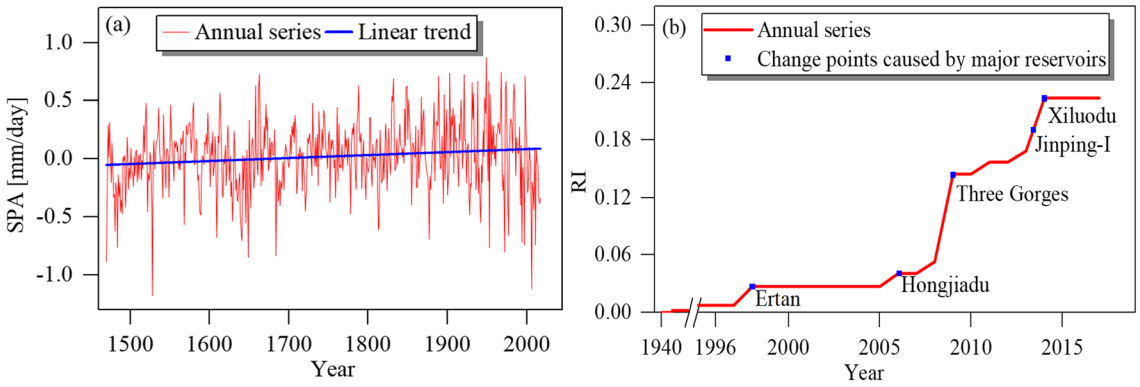

Figure 4. Interannual variation of (a) the summer precipitation anomaly (SPA) and (b) the reservoir index (RI) in the upper Yangtze River basin (the major reservoirs increasing the RI have been marked).

provided by Bureau of Hydrology, CWRC. The historical flood data include the six largest historical floods since 1470 shown in Table 2 and the unknown floods below 80,000 m^3/s.

3.4. Uncertainty Scenario for the Historical Data of Both Covariates and Flood

In this study, the uncertainty in the historical data was considered in assessing the robustness of flood estimation. The RI in the historical period from 1470 to 1881 is equal to zero. It is not required to consider its uncertainty. Thus, only the uncertainty for precipitation and flood data were considered. To investigate the effects of historical data uncertainty on flood estimation, based on Equations 6 and 11, six uncertainty scenarios (S0, S1, S2, S3, S4, and S5) were designed by certain standard deviations of random errors associated with the AMDF of the six known historical floods, the CT of the unknown historical floods, and the SPA during the historical period (1470–1881), as shown in Table 3. The standard deviations of errors associated with those AMDF and SPA are assumed to be the 0%, 10%, 30%, or 50% of the standard deviations of the AMDF and SPA samples, respectively, while the standard deviation of errors associated with the CT is assumed to be the 0% or 10% of the fixed CT value. Then, combining the six uncertainty scenarios, the SGEV_CD model has six types, denoted as SGEV_CD_S0, SGEV_CD_S1, SGEV_CD_S2, SGEV_CD_S3, SGEV_CD_S4, and SGEV_CD_S5. The similar naming scheme is for the NGEV_CD model.

3.5. Results

3.5.1. Preliminary Analysis

Figure 4 shows the interannual variations of covariates across the study area. For the SPA (Figure 4a), the slight increase trend and periodic fluctuation occur over the entire period, but the significant decrease trend occurs over the period 1882–2017, especially over the period 1998–2017. Figure 4b shows that the RI has been increased significantly, due to the construction of many reservoirs since 1998. The RI value reached

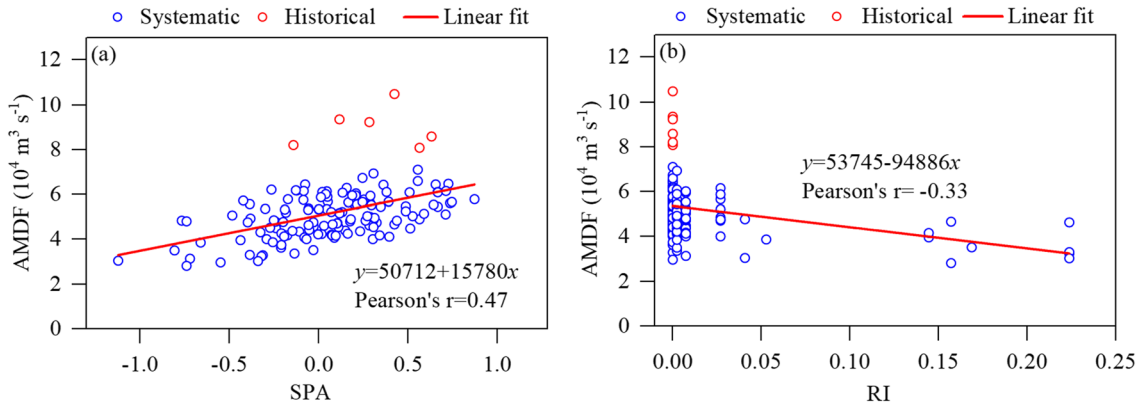

Figure 5. Scatterplots between the observed AMDF and the corresponding values of (a) the SPA and (b) the RI in the upper Yangtze River basin.

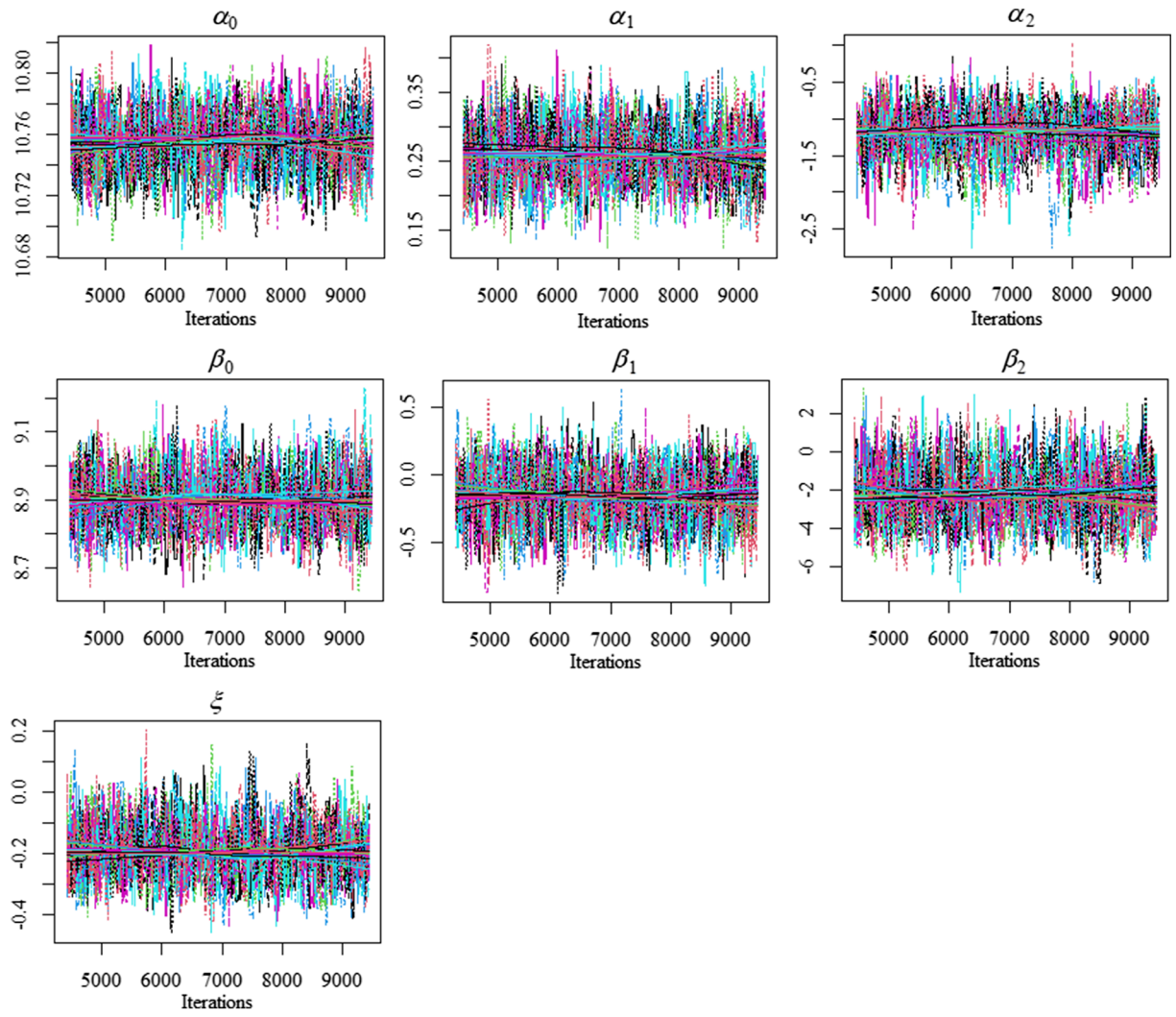

Figure 6. Trace plots with the last 5,000 iterations from the DiffeRential Evolution Adaptive Metropolis (DREAM) simulation using 14 interacting chains for parameter estimation of the global NGEV_SD model ($\mu_t = \exp(\alpha_0 + \alpha_1 \mathrm{SPA} + \alpha_2 \mathrm{RI})$, $\sigma_t = \exp(\beta_0 + \beta_1 \mathrm{SPA} + \beta_2 \mathrm{RI})$, $\xi_t = \xi$).

Table 4
Priors and Posteriors of the Seven Parameters for Sampling in the Global NGEV_SD Model ($\mu_t = exp(\alpha_0+\alpha_1 SPA + \alpha_2 RI)$, $\sigma_t = exp(\beta_0 + \beta_1 SPA+ \beta_2 RI)$, $\xi_t = \xi$)

Model parameters	Prior distribution	Posterior mean	Posterior standard deviation
α_0	$N(9,5)$	10.7	0.295
α_1	$N(0,5)$	0.310	0.386
α_2	$N(0,5)$	−0.982	1.52
β_0	$N(9,5)$	8.93	0.240
β_1	$N(0,5)$	−0.165	0.203
β_2	$N(0,5)$	−2.33	1.45
ξ	$U(-0.5,0.5)$	−0.202	0.0933

Note. NGEV_SD indicates nonstationary models based on the generalized extreme value distribution given the systematic data. *N* is the normal distribution with mean and standard deviation in parentheses; and *U* is the uniform distribution with range in parentheses.

0.22 in 2017, indicating the large effects of upstream reservoirs on the hydrological regimes of the Yichang gauging station.

Figure 5 illustrates that there is the Pearson correlation of 0.47 between AMDF and the SPA (Figure 5a), while there is the Pearson correlation of −0.33 between AMDF and the RI (Figure 5b). This indicates that AMDF has a significant linear correlation with each of both SPA and RI. Thus, it can be inferred that the incorporation of the two covariates into the NGEV models possibly improves the accuracy of flood modeling. Note that the historical floods are displaying departures from the linear regression line in Figure 5a. The possible explanation for this heteroscedasticity is that in addition to the SPA, which is a climate indicator in seasonal scale, there must be some other unknown or unaccounted factors (e.g., the temporal and spatial distribution of rainfall in extreme cases) that would combine together to affect the AMDF.

3.5.2. Model Parameter Computation Using an MCMC Algorithm

According to the models developed in section 2, the number of model parameters to be estimated in this case study is between three and

Table 5
Model Specification, Deviance Information Criterion (DIC), the Posterior Mean of Deviance ($\overline{D}$), and the Deviance at the Posterior Parameter Mean ($\widehat{D}$) in Covariate Selection Analysis for the NGEV_SD Models (i.e., the Nonstationary Models Based on the Generalized Extreme Value Distribution Given the Systematic Data)

		$g_1(\mu_t) = \mu_t$			$g_1(\mu_t) = \ln(\mu_t)$		
Candidates		DIC	$\overline{D}$	$\widehat{D}$	DIC	$\overline{D}$	$\widehat{D}$
1[a]	$g_1(\mu_t)$~1,ln(σ_t)~1	2,872.5	2,869.7	2,867.0	2,872.3	2,869.6	2,867.0
2	$g_1(\mu_t)$~SPA,ln(σ_t)~1	2,826.2	2,822.4	2,818.7	2,827.5	2,823.7	2,819.8
3	$g_1(\mu_t)$~RI,ln(σ_t)~1	2,851.9	2,848.3	2,844.8	2,851.3	2,847.5	2,843.7
4	$g_1(\mu_t)$~1,ln(σ_t)~SPA	2,874.0	2,870.6	2,867.1	2,874.4	2,870.7	2,867.1
5	$g_1(\mu_t)$~1,ln(σ_t)~RI	2,870.9	2,867.3	2,863.7	2,871.3	2,867.5	2,863.8
6	$g_1(\mu_t)$~SPA+RI,ln(σ_t)~1	2,814.1	2,809.5	2,804.9	2,818.8	2,812.6	2,806.5
7	$g_1(\mu_t)$~SPA,ln(σ_t)~SPA	2,825.9	2,821.3	2,816.7	2,831.4	2,824.7	2,818.1
8	$g_1(\mu_t)$~SPA,ln(σ_t)~RI	2,827.5	2,822.8	2,818.2	2,829.8	2,824.6	2,819.3
9	$g_1(\mu_t)$~RI,$g_2(\sigma_t)$~SPA	2,853.5	2,849.2	2,844.9	2,853.4	2,848.6	2,843.8
10	$g_1(\mu_t)$~RI,$g_2(\sigma_t)$~RI	2,852.1	2,847.8	2,843.4	2,852.0	2,847.4	2,842.8
11	$g_1(\mu_t)$~1,ln(σ_t)~SPA+RI	2,873.0	2,868.3	2,863.6	2,873.5	2,868.6	2,863.8
12	$g_1(\mu_t)$~SPA+RI,$g_2(\sigma_t)$~SPA	2,816.8	2,810.8	2,804.8	2,822.5	2,814.4	2,806.3
13[b]	$g_1(\mu_t)$~SPA+RI,$g_2(\sigma_t)$~RI	**2,811.3**	**2,805.8**	2,800.3	**2,817.4**	**2,810.2**	2,803.0
14	$g_1(\mu_t)$~SPA,$g_2(\sigma_t)$~SPA+RI	2,828.6	2,822.7	2,816.7	2,833.9	2,826.2	2,818.6
15	$g_1(\mu_t)$~RI,$g_2(\sigma_t)$~SPA+RI	2,853.9	2,848.7	2,843.5	2,854.8	2,849.0	2,843.2
16[c]	$g_1(\mu_t)$~SPA+RI,$g_2(\sigma_t)$~SPA+RI	2,813.6	2,806.7	**2,799.8**	2,818.8	2,810.5	**2,802.3**

Note. The value in bold font is the lowest value for the same criterion.
[a]Stationary (classical) model without any covariate. [b]Optimal model in covariate selection based on DIC. [c]Global model in covariate selection.

seven. The global NGEV_SD model with seven parameters and an exponential formula for calculating μ_t is used to illustrate how the model parameters are computed under the Bayesian framework, which is expressed by

$$\begin{aligned} \mu_t &= \exp(\alpha_0 + \alpha_1 \mathrm{SPA} + \alpha_2 \mathrm{RI}), \\ \sigma_t &= \exp(\beta_0 + \beta_1 \mathrm{SPA} + \beta_2 \mathrm{RI}), \\ \xi_t &= \xi. \end{aligned} \tag{17}$$

A suitable MCMC algorithm for sampling is important to form a stationary and ergodic posterior distribution in the relative high dimension. The DiffeRential Evolution Adaptive Metropolis (DREAM) algorithm (Laloy & Vrugt, 2012; Vrugt et al., 2009) is an efficient MCMC method. Based on a self-adaptive Differential Evolution strategy, the DREAM can run multiple interacting chains to globally explore the posterior distribution. In the case study, the posterior distribution is computed by the aid of the DREAM(zs) function in the R package "BayesianTools" (Hartig et al., 2019). The start parameter values are sampled by a fat prior. The chain number is equal to the double of the parameter dimension. And we run at least 10,000 iterations (the burn-in consists of 2,000 iterations) for each chain.

Figure 6 shows the trace plots with the last 5,000 iterations from the DREAM simulation using 14 interacting chains for parameter estimation of the global NGEV_SD model by Equation 17. The trace plots indicate that the chains have been stationary for all model parameters. The priors and posteriors of the seven parameters are displayed in Table 4.

3.5.3. Covariate Selection Analysis of the NGEV_SD Models

In the NGEV_SD models, there are 16 linear combinations in the two-covariate case for both distribution parameters, as well as two candidate functions for calculating μ_t (as shown in Equation 3).

Table 5 presents the criteria of all NGEV_SD models. It is found that in terms of the same criteria, there is tiny difference between identity and logarithmic functions for calculating μ_t, and the identity function is preferred. The global model has the lowest deviance at the parameter posterior mean, but this model is not selected due to larger posterior mean of deviance. Then the $^{\mathrm{opt}}$NGEV_SD model with the lowest DIC value of 2,811.3 is

Water Resources Research

10.1029/2020WR027112

Table 6
Parameter Posterior Means, With the Posterior Standard Deviations in Parentheses, Deviance Information Criterion (DIC) of Various Models in the Study Area

Models	Formulas for calculating distribution parameters	Estimates of model parameters						DIC
		$\widehat{\alpha}_0$	$\widehat{\alpha}_1$	$\widehat{\alpha}_2$	$\widehat{\beta}_0$	$\widehat{\beta}_1$	$\widehat{\xi}$	
SGEV_SD	$\mu_t = \alpha_0$	46,909.6	—	—	9.16	—	−0.33	2,872.5
	$\sigma_t = \exp(\beta_0)$	(1,037.2)			(0.11)		(0.052)	
SGEV_CD_S3	$\xi_t = \xi$	45,893.4	—	—	9.13	—	−0.087	3,086.9
		(954.3)			(0.26)		(0.030)	
^{opt}NGEV_SD	$\mu_t = \alpha_0 + \alpha_1 \mathrm{SPA} + \alpha_2 \mathrm{RI}$	47,017.1	12,623.1	−44,330.9	8.89	−2.41	−0.20	2,811.3
	$\sigma_t = \exp(\beta_0 + \beta_1 \mathrm{RI})$	(999.6)	(2,329.3)	(9,767.9)	(0.16)	(1.30)	(0.082)	
^{opt}NGEV_CD_S3	$\xi_t = \xi$	46,507.3	13,535.4	−43,856.7	8.88	−3.92	0.0035	3,006.8
		(939.8)	(1,633.8)	(8,280.3)	(0.25)	(1.47)	(0.042)	

Note. SGEV_SD is the stationary model given the systematic data; SGEV_CD_S3 is the stationary model given the censored data with the representative uncertainty scenario (S3); ^{opt}NGEV_SD is the optimal nonstationary model given the systematic data; and ^{opt}NGEV_CD_S3 is the optimal nonstationary model given the censored data with the representative uncertainty scenario (S3).

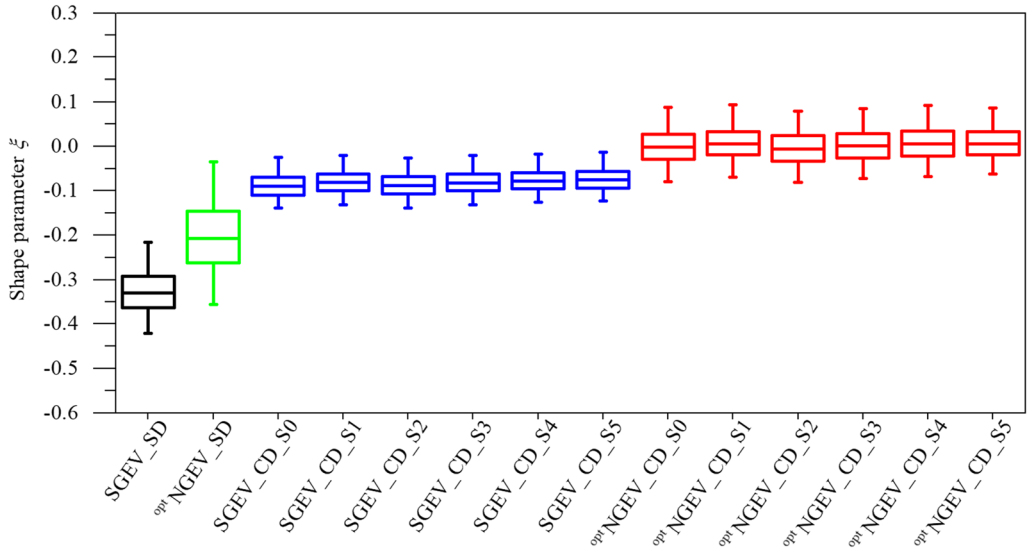

SGEV_SD is the stationary model given the systematic data;

SGEV_SD_Si is the stationary model given the censored data under different uncertainty scenarios (Si, $i = 0,1,\ldots,5$);

^{opt}NGEV_SD is the optimal nonstationary model given the systematic data;

^{opt}NGEV_CD_Si is the optimal nonstationary model given the censored data under different uncertainty scenarios (Si, $i = 0,1,\ldots,5$).

Figure 7. Posterior distributions of the shape parameter ξ in the various models. SGEV_SD is the stationary model given the systematic data; SGEV_SD_Si is the stationary model given the censored data under different uncertainty scenarios (Si, $i = 0,1,\ldots,5$); ^{opt}NGEV_SD is the optimal nonstationary model given the systematic data; and ^{opt}NGEV_CD_Si is the optimal nonstationary model given the censored data under different uncertainty scenarios (Si, $i = 0,1,\ldots,5$).

$$\begin{aligned} \mu_t &= \alpha_0 + \alpha_1 \mathrm{SPA} + \alpha_2 \mathrm{RI}, \\ \sigma_t &= \exp(\beta_0 + \beta_1 \mathrm{RI}), \\ \xi_t &= \xi. \end{aligned} \tag{18}$$

3.5.4. Comparison of the SGEV_SD, SGEV_CD, NGEV_SD, and NGEV_CD Models

In order to compare the models (SGEV_SD, SGEV_CD, NGEV_SD, and NGEV_CD) clearly, we selected the representative scenario (S3) which contains a small uncertainty for the historical data. In the nonstationary models, the optimal formulas of two distribution parameters, μ_t and σ_t, are given by Equation 18. The results of Bayesian parameter estimation for the models (SGEV_SD, SGEV_CD_S3, ^{opt}NGEV_SD, and ^{opt}NGEV_CD_S3) were summarized in Table 6. First, the DIC (2,811.3) of the NGEV_SD model is lower than that (2,872.5) of the SGEV_SD model, and the DIC (3,006.8) of the ^{opt}NGEV_CD_S3 model is lower than that (3,086.9) of the SGEV_CD_S3 model. It is indicated that the nonstationary models (^{opt}NGEV_SD and ^{opt}NGEV_CD_S3) are preferred. Second, the shape parameter estimates $\widehat{\xi}$ between the SGEV_CD_S3 and SGEV_SD models, with −0.087 and −0.33, are significantly different, whereas the other parameter estimates ($\widehat{\alpha}_0$ and $\widehat{\beta}_0$) between the two models are close. The situation is similar for NGEV_CD_S3 and NGEV_SD models. It is suggested that regardless of stationary model or nonstationary model, flood data type results in a significant impact on the shape parameter (ξ) which controls the tail of probability distribution, whereas a slight impact on the other model parameters ($\boldsymbol{\alpha}$ and $\boldsymbol{\beta}$).

The impacts of data type and historical data uncertainty on the shape parameter are investigated further. Figure 7 shows the posterior distributions of the shape parameter ξ in the various models. Under the same assumption condition (either stationary or nonstationary), the models based the CD bring a higher posterior mean and a smaller posterior standard deviation. Estimates of the shape parameter from the models (SGEV_CD_S0, SGEV_CD_S1, SGEV_CD_S2, SGEV_CD_S3, SGEV_CD_S4, and SGEV_CD_S5)

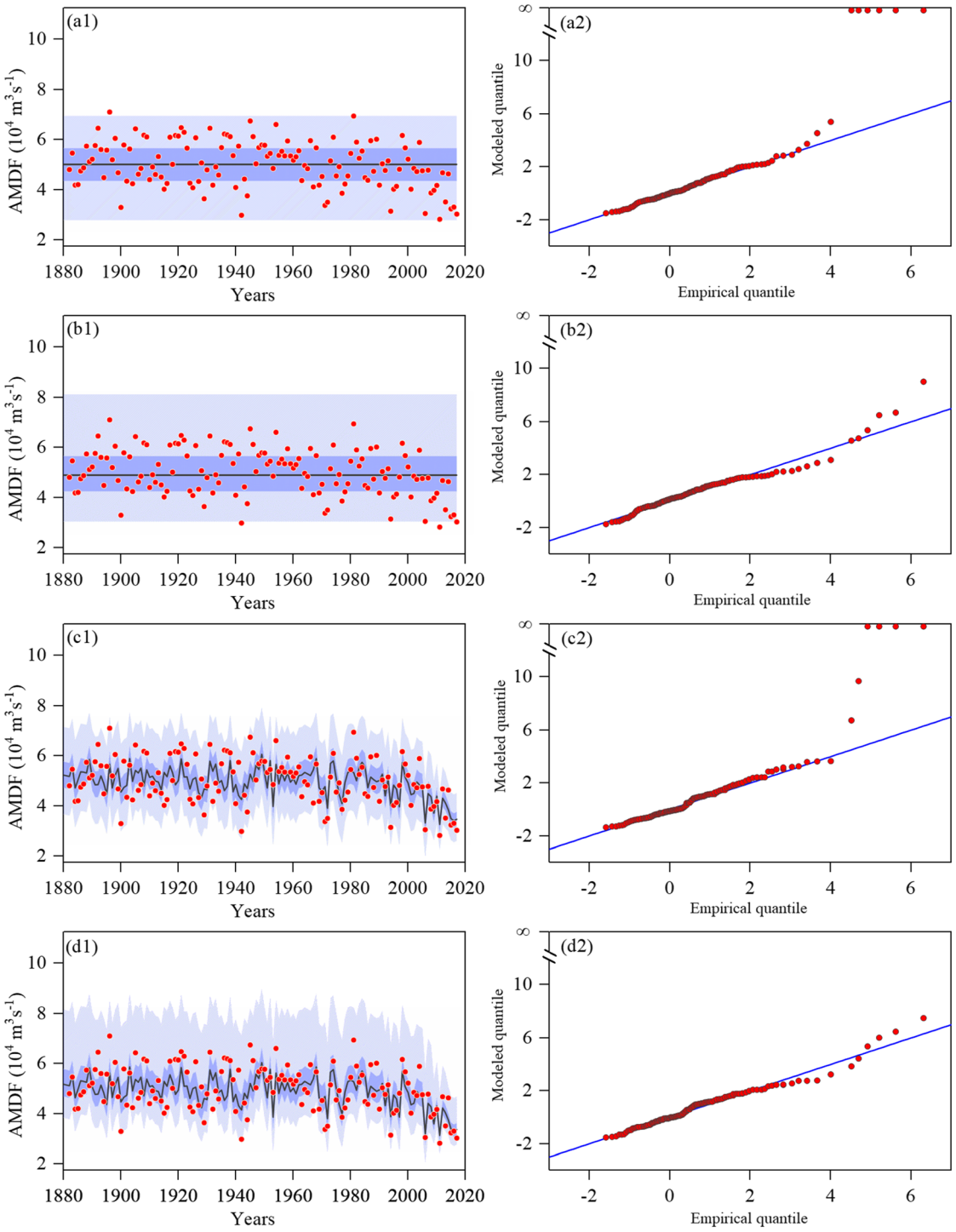

Figure 8. Performance of (a) the SGEV_SD model, (b) the SGEV_CD_S3 model, (c) the ^{opt}NGEV_SD model, and (d) the ^{opt}NGEV_CD_S3 model. The left panels (a1, b1, c1, and d1) are the centile curves plots (the 50th centile curves are indicated by the black lines; the light blue-filled areas are between the 1st and 99th centile curves; the dark blue-filled areas are between the 25th and 75th centile curves; the systematic data are indicated by the filled red points). The right panels (a2, b2, c2, and d2) are the standard residual quantile plots (note that the six historical floods are also checked) on the Gumbel scale; a good model should have the plotted points close to 1:1 blue lines.

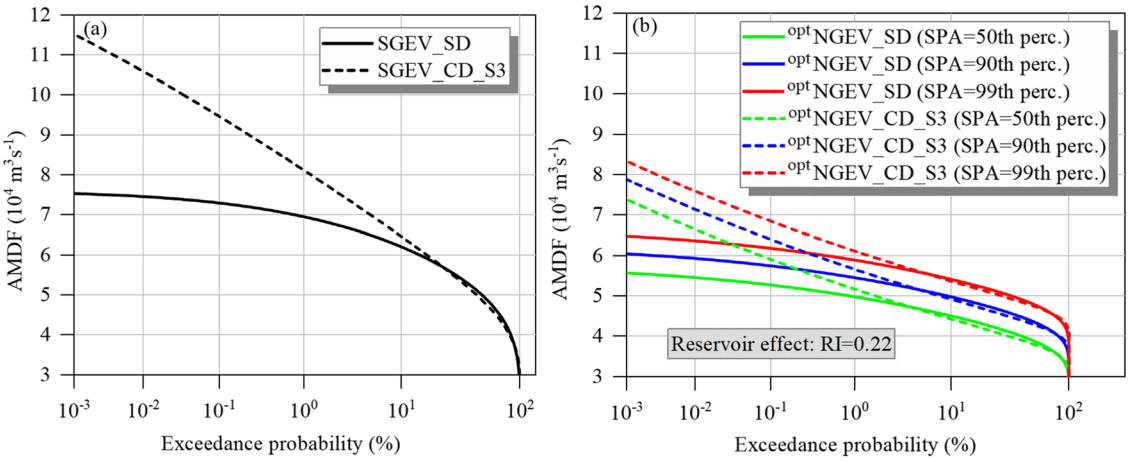

Figure 9. Tails of cumulative probability distributions given by (a) the stationary models (SGEV_SD and SGEV_CD_S3) and (b) the nonstationary models (^{opt}NGEV_SD and ^{opt}NGEV_CD_S3) with the RI of 0.22 and with the SPA of the 50th, 90th, and 99th percentiles.

have little difference. The same situation occurs in the nonstationary models (^{opt}NGEV_CD_S0, ^{opt}NGEV_CD_S1, ^{opt}NGEV_CD_S2, ^{opt}NGEV_CD_S3, ^{opt}NGEV_CD_S4, and ^{opt}NGEV_CD_S5). It is inferred that if only the historical data uncertainty is not very large, its impact may be limited. Besides, it is found that given the same set of flood data (either the SD or CD), the results of the nonstationary models have a higher posterior mean and a larger uncertainty in the estimation of parameter ξ than stationary model.

The performance of models (SGEV_SD, SGEV_CD_S3, ^{opt}NGEV_SD, and ^{opt}NGEV_CD_S3) is checked to obtain the final model. The centile curves plots (Figures 8a1–8d1) suggest that the magnitude of floods has been decreased since 1998. Most observed points since 1998 are below the 50th centile curves provided by the SGEV_SD and SGEV_CD_S3 models (Figures 8a1 and 8b1), whereas all the observed points are uniformly distributed over the estimated centiles range provided by the ^{opt}NGEV_SD and ^{opt}NGEV_CD_S3 models (Figures 8c1 and 8d1). It is indicated that compared to the stationary models (SGEV_SD and SGEV_CD_S3), the nonstationary models (NGEV_SD and NGEV_CD_S3) are able to capture the variation of the SD and provide a good fit to the SD, due to the incorporation of covariates (SPA and RI). Besides, Figures 8c1 and 8d1 also show that since 1998, the location and scale of the GEV distribution are decreasing, resulting from the increasing RI. Figures 8a2–8d2 illustrate the standard residual quantile plots of the SGEV_SD, SGEV_CD_S3, ^{opt}NGEV_SD, and ^{opt}NGEV_CD_S3 models on the Gumbel scale. Note that six historical floods are also checked. Some unreasonable points arose in the SGEV_SD and ^{opt}NGEV_SD models (Figures 8a2 and 8c2), which means that when the historical data are not incorporated, some historical floods will be treated as the impossible events. For the SGEV_CD_S3 and ^{opt}NGEV_CD_S3 models (Figures 8b2 and 8d2), all points are close to the 1:1 lines, but the situation for the ^{opt}NGEV_CD_S3 model is obviously better.

Figure 9 illustrates the tails of cumulative probability distributions provided by the models (SGEV_SD, SGEV_CD_S3, ^{opt}NGEV_SD, and ^{opt}NGEV_CD_S3) with the RI of 0.22 and with the SPA of the 50th, 90th, and 99th percentiles. Figure 9a shows that when the exceedance probability is over 10%, the flood estimates between the SGEV_SD and SGEV_CD_S3 models are close, but when the exceedance probability is less 10%, the flood estimates are significantly different. And the SGEV_CD_S3 model has a larger estimate in the tail. Figure 9b shows that given the same values of covariates, a similar situation occurs in the NGEV_SD and NGEV_CD_S3 models. It is indicated that in the case area, the historical data just change the tail behavior regardless of the stationary models or nonstationary models. Besides, compared to the stationary models (Figure 9a), the nonstationary models (Figure 9b) have lower curves, since the reservoir-induced nonstationarity has been considered with RI = 0.22.

The uncertainty of flood quantiles given by the stationary and nonstationary models can be calculated based on the empirical posterior distribution of model parameters and given the values of covariates. Figure 10 shows the 95% uncertainty interval of the tails of cumulative probability distributions given by the

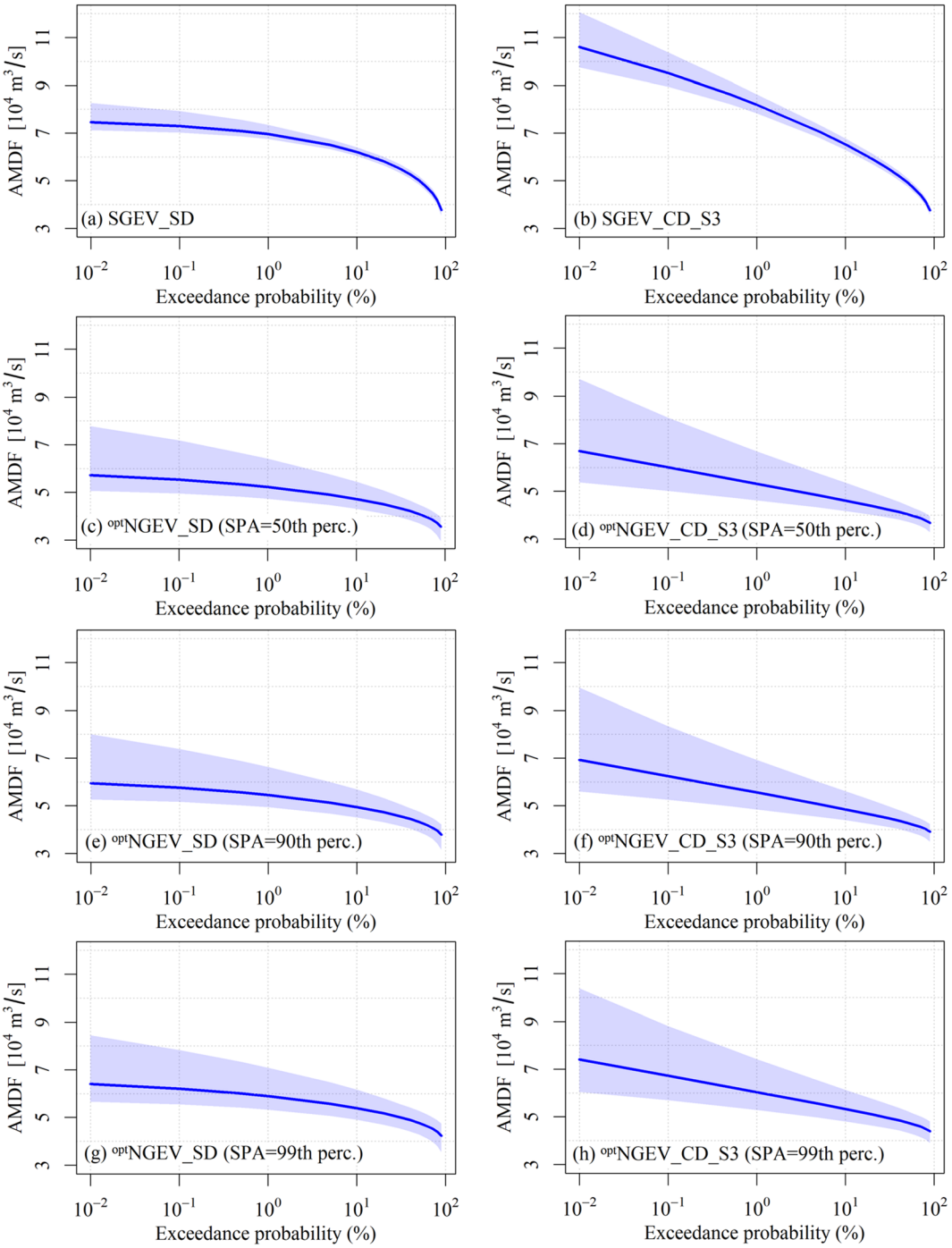

Figure 10. 95% uncertainty interval (light blue-filled area) of the tails of cumulative probability distributions given by the stationary models (SGEV_SD and SGEV_CD_S3) and the nonstationary models (^{opt}NGEV_SD and ^{opt}NGEV_CD_S3) with the RI of 0.22 and with the SPA of the 50th, 90th, and 99th percentiles.

SGEV_SD, SGEV_CD, ^{opt}NGEV_SD, and ^{opt}NGEV_CD_S3 models with the RI of 0.22 and with the SPA of the 50th, 90th, and 99th percentiles. The width of the uncertainty intervals indicates that the results of the nonstationary models have a larger uncertainty than the stationary models; on the other hand, the uncertainty in the results of the nonstationary models is located in an acceptable range.

4. Conclusions and Discussions

Both the nonstationarity and the data length have a vital impact on the accuracy of design flood estimates in flood frequency analysis. This paper established the framework of nonstationary flood frequency analysis with the ability to utilize the CD (i.e., the combination of the systematic and historical data), as well as to consider both the historical data uncertainty and the model parameter uncertainty. Compared with the SD, the CD contain additional information, that is, the historical data. The usefulness of historical flood information under the nonstationary flood frequency analysis framework may be remarkable to reduce the uncertainty, especially for the tail estimation. In the case study, both the (climate-induced and reservoir-induced) nonstationarity and the historical information were considered. It is demonstrated that the SPA and RI are the remarkable variables for explaining the interannual variation of downstream flood in the study area, and for the same set of flood data (either SD or CD), the nonstationary models are preferred to the stationary ones according to the DIC and the goodness-of-fit check. It is also demonstrated that regardless of the stationary models or nonstationary models, the temporal information expansion results in a higher posterior mean and a smaller uncertainty for the shape parameter which controls the tail of the GEV distribution. Other major findings are listed as follows:

1. The interannual variation of the SPA and the RI from 1470 to 2017 across the study area indicates that the SPA has periodic fluctuation characteristics and a slightly increasing trend, and the RI has been impressively increased since 1998. And each of the above two covariates has a significant linear correlation with the AMDF.
2. The results of model parameters suggest that the addition of the historical flood data significantly affects the shape parameter and slightly affects those model parameters in the formulas for calculating the location and scale parameters.
3. In terms of the optimized results of the shape parameter, there are few differences between six uncertainty scenarios for the historical flood and covariate data. It is suggested that the small errors in determining the values of historical floods might not have substantial impact on the design flood value in this case study. Of course, more scenarios can be designed and investigated if more concrete information about the historical data is available.
4. Since 1998, the magnitude of the AMDF has been in a decreasing trend. The stationary models are unable to capture the nonstationarity of the AMDF series, whereas the nonstationary models can perform well.
5. According to the performance of the nonstationary models (^{opt}NGEV_SD and ^{opt}NGEV_CD_S3), the ^{opt}NGEV_SD model fits the SD of floods well but could not fit the historical flood data well, while the ^{opt}NGEV_CD_S3 model can fit both the SD and the historical data well. It is indicated that under the nonstationary condition, the temporal information expansion may be valuable to correct the probability estimation for the rare flood events in the case study.

In summary, the covariate-based nonstationary flood frequency analysis of the CD in the upper Yangtze River basin, China, suggests that the incorporation of richer sample information of floods and/or covariate information is worth effort. In terms of the uncertainty associated with model parameters, all models in the case study seem to be practical. In practice, the application of the NGEV models to nonstationary hydrologic design should be careful, considering the additional uncertainty introduced by the more complex model structures (Milly et al., 2015; Montanari & Koutsoyiannis, 2014; Serinaldi & Kilsby, 2015). It is recommended that the hydrological designers should comprehensively consider the impacts of climate change, human activity, and historical flood events in flood frequency analysis, as the flood frequency models with different considerations might lead to the remarkable differences in estimated flood quantiles, as has been shown in this study.

Data Availability Statement

Precipitation reconstruction data are available online (on https://www.ncdc.noaa.gov/paleo/study/23056). Precipitation gauge data are collected by the National Climate Center of the China Meteorological Administration and available on http://data.cma.cn/data/cdcdetail/dataCode/SURF_CLI_CHN_MUL_DAY_V3.0.html under request. Streamflow data are collected by Bureau of Hydrology, Changjiang Water Resources Commission, China, and available under request.

Acknowledgments

The study is financially supported jointly by the National Natural Science Foundation of China (41890822 and 51525902), the Research Council of Norway (FRINATEK Project 274310), and the Ministry of Education "Plan 111" Fund of China (B18037), all of which are greatly appreciated. We greatly appreciate the editor and the two reviewers for their insightful comments and constructive suggestions for improving the manuscript.

References

Batalla, R. J., Gomez, C. M., & Kondolf, G. M. (2004). Reservoir-induced hydrological changes in the Ebro River basin (NE Spain). *Journal of Hydrology*, *290*(1–2), 117–136. https://doi.org/10.1016/j.jhydrol.2003.12.002

Bayliss, A., & Reed, D. W. (2001). *The use of historical data in flood frequency estimation: Report to MAFF*. Wallingford, KY: Centre for Ecology and Hydrology. Retrieved from http://nora.nerc.ac.uk/id/eprint/8060/1/BaylissRepN008060CR.pdf

Brázdil, R., Kiss, A., Luterbacher, J., Nash, D. J., & Řezníčková, L. (2018). Documentary data and the study of past droughts: A global state of the art. *Climate of the Past*, *14*(12), 1915–1960. https://doi.org/10.5194/cp-14-1915-2018

Brázdil, R., Řezníčková, L., Valášek, H., Havlíček, M., Dobrovolný, P., Soukalová, E., et al. (2011). Fluctuations of floods of the River Morava (Czech Republic) in the 1691–2009 period: Interactions of natural and anthropogenic factors. *Hydrological Sciences Journal–Journal des Sciences Hydrologiques*, *56*(3), 468–485. https://doi.org/10.1080/02626667.2011.564175

Changjiang Water Resources Commission (CWRC). (1996). *Hydrologic inscription cultural relics in Three Gorges Reservoir (in Chinese)*. Beijing, China: Science Press.

Coles, S. (2001). *An introduction to statistical modeling of extreme values*. London, England: Springer. https://doi.org/10.1007/978-1-4471-3675-0

De Paola, F., Giugni, M., Pugliese, F., Annis, A., & Nardi, F. (2018). GEV parameter estimation and stationary vs. non-stationary analysis of extreme rainfall in African test cities. *Hydrology*, *5*(2), 28. https://doi.org/10.3390/hydrology5020028

Du, T., Xiong, L., Xu, C. Y., Gippel, C. J., Guo, S., & Liu, P. (2015). Return period and risk analysis of nonstationary low-flow series under climate change. *Journal of Hydrology*, *527*, 234–250. https://doi.org/10.1016/j.jhydrol.2015.04.041

El Adlouni, S., Ouarda, T. B., Zhang, X., Roy, R., & Bobée, B. (2007). Generalized maximum likelihood estimators for the nonstationary generalized extreme value model. *Water Resources Research*, *43*, W03410. https://doi.org/10.1029/2005WR004545

England, J. F., Cohn, T. A., Faber, B. A., Stedinger, J. R., Thomas, W. O., Veilleux, A. G., et al. (2019). *Guidelines for determining flood flow frequency—Bulletin 17C (ver. 1.1, May 2019), U.S. Geological Survey Techniques and Methods* (Book 4, Ch. B5, p. 148). Reston, VA: U.S. Geological Survey. https://doi.org/10.3133/tm4B5

Gao, B., Yang, D., & Yang, H. (2013). Impact of the Three Gorges Dam on flow regime in the middle and lower Yangtze River. *Quaternary International*, *304*, 43–50. https://doi.org/10.1016/j.quaint.2012.11.023

Gilroy, K. L., & McCuen, R. H. (2012). A nonstationary flood frequency analysis method to adjust for future climate change and urbanization. *Journal of Hydrology*, *414-415*, 40–48. https://doi.org/10.1016/j.jhydrol.2011.10.009

Guo, S. L., & Cunnane, C. (1991). Evaluation of the usefulness of historical and palaeological floods in quantile estimation. *Journal of Hydrology*, *129*(1–4), 245–262. https://doi.org/10.1016/0022-1694(91)90053-K

Hartig, F., Minunno, F., & Paul, S. (2019). BayesianTools: General-purpose MCMC and SMC samplers and tools for Bayesian statistics. *R package version 0.1.7*. Retrieved from https://CRAN.R-project.org/package=BayesianTools

Hua, T., Zorita, E., Wang, X., Wang, N., & Zhang, C. (2019). Precipitation variability in the north fringe of East Asian Summer Monsoon during the past millennium and its possible driving factors. *Climate Dynamics*, *53*(5-6), 2587–2602. https://doi.org/10.1007/s00382-019-04643-1

Jiang, C., Xiong, L., Wang, D., Liu, P., Guo, S., & Xu, C. Y. (2015). Separating the impacts of climate change and human activities on runoff using the Budyko-type equations with time-varying parameters. *Journal of Hydrology*, *522*, 326–338. https://doi.org/10.1016/j.jhydrol.2014.12.060

Jiang, C., Xiong, L., Yan, L., Dong, J., & Xu, C. Y. (2019). Multivariate hydrologic design methods under nonstationary conditions and application to engineering practice. *Hydrology and Earth System Sciences*, *23*(3), 1683–1704. https://doi.org/10.5194/hess-23-1683-2019

Katz, R. W., Parlange, M. B., & Naveau, P. (2002). Statistics of extremes in hydrology. *Advances in Water Resources*, *25*(8–12), 1287–1304. https://doi.org/10.1016/S0309-1708(02)00056-8

Kjeldsen, T. R., Macdonald, N., Lang, M., Mediero, L., Albuquerque, T., Bogdanowicz, E., et al. (2014). Documentary evidence of past floods in Europe and their utility in flood frequency estimation. *Journal of Hydrology*, *517*, 963–973. https://doi.org/10.1016/j.jhydrol.2014.06.038

Kwon, H. H., Brown, C., & Lall, U. (2008). Climate informed flood frequency analysis and prediction in Montana using hierarchical Bayesian modeling. *Geophysical Research Letters*, *35*, L05404. https://doi.org/10.1029/2007GL032220

Laloy, E., & Vrugt, J. A. (2012). High-dimensional posterior exploration of hydrologic models using multiple-try $\text{DREAM}_{(ZS)}$ and high-performance computing. *Water Resources Research*, *48*, W01526. https://doi.org/10.1029/2011WR010608

Li, J., Liu, X., & Chen, F. (2015). Evaluation of nonstationarity in annual maximum flood series and the associations with large-scale climate patterns and human activities. *Water Resources Management*, *29*(5), 1653–1668. https://doi.org/10.1007/s11269-014-0900-z

Li, Q., Peng, J., & Shen, Y. (2012). Development of China homogenized monthly precipitation dataset during 1900–2009. *Journal of Geographical Sciences*, *22*(4), 579–593. https://doi.org/10.1007/s11442-012-0948-8

Li, T., Guo, S., Chen, L., & Guo, J. (2013). Bivariate flood frequency analysis with historical information based on copula. *Journal of Hydrologic Engineering*, *18*(8), 1018–1030. https://doi.org/10.1061/%28ASCE%29HE.1943-5584.0000684

Liu, D., Guo, S., Lian, Y., Xiong, L., & Chen, X. (2015). Climate-informed low-flow frequency analysis using nonstationary modelling. *Hydrological Processes*, *29*(9), 2112–2124. https://doi.org/10.1002/hyp.10360

López, J., & Francés, F. (2013). Non-stationary flood frequency analysis in continental Spanish rivers, using climate and reservoir indices as external covariates. *Hydrology and Earth System Sciences*, *17*(8), 3189–3203. https://doi.org/10.5194/hess-17-3189-2013

Lu, F., Song, X., Xiao, W., Zhu, K., & Xie, Z. (2020). Detecting the impact of climate and reservoirs on extreme floods using nonstationary frequency models. *Stochastic Environmental Research and Risk Assessment*, *34*(1), 169–182. https://doi.org/10.1007/s00477-019-01747-2

Machado, M. J., Botero, B. A., López, J., Francés, F., Díez-Herrero, A., & Benito, G. (2015). Flood frequency analysis of historical flood data under stationary and non-stationary modelling. *Hydrology and Earth System Sciences*, *19*(6), 2561–2576. https://doi.org/10.5194/hess-19-2561-2015

Macklin, M. G., & Lewin, J. (2008). Alluvial responses to the changing Earth system. *Earth Surface Processes and Landforms*, *33*(9), 1374–1395. https://doi.org/10.1002/esp.1714

Martins, E. S., & Stedinger, J. R. (2000). Generalized maximum-likelihood generalized extreme-value quantile estimators for hydrologic data. *Water Resources Research*, *36*(3), 737–744. https://doi.org/10.1029/1999WR900330

Merz, R., & Blöschl, G. (2008a). Flood frequency hydrology: 1. Temporal, spatial, and causal expansion of information. *Water Resources Research*, *44*, W08432. https://doi.org/10.1029/2007WR006744

Merz, R., & Blöschl, G. (2008b). Flood frequency hydrology: 2. Combining data evidence. *Water Resources Research*, *44*, W08433. https://doi.org/10.1029/2007WR006745

Milly, P. C., Betancourt, J., Falkenmark, M., Hirsch, R. M., Kundzewicz, Z. W., Lettenmaier, D. P., & Stouffer, R. J. (2008). Stationarity is dead: Whither water management? *Science*, *319*(5863), 573–574. https://doi.org/10.1126/science.1151915

Milly, P. C., Betancourt, J., Falkenmark, M., Hirsch, R. M., Kundzewicz, Z. W., Lettenmaier, D. P., et al. (2015). On critiques of "Stationarity is dead: Whither water management?". *Water Resources Research*, *51*, 7785–7789. https://doi.org/10.1002/2015WR017408

Montanari, A., & Koutsoyiannis, D. (2014). Modeling and mitigating natural hazards: Stationarity is immortal! *Water Resources Research*, *50*, 9748–9756. https://doi.org/10.1002/2014WR016092

Ouarda, T. B. M. J., & El-Adlouni, S. (2011). Bayesian nonstationary frequency analysis of hydrological variables 1. *Journal of the American Water Resources Association*, *47*(3), 496–505. https://doi.org/10.1111/j.1752-1688.2011.00544.x

Parkes, B., & Demeritt, D. (2016). Defining the hundred year flood: A Bayesian approach for using historic data to reduce uncertainty in flood frequency estimates. *Journal of Hydrology*, *540*, 1189–1208. https://doi.org/10.1016/j.jhydrol.2016.07.025

Payrastre, O., Gaume, E., & Andrieu, H. (2011). Usefulness of historical information for flood frequency analyses: Developments based on a case study. *Water Resources Research*, *47*, W08511. https://doi.org/10.1029/2010WR009812

Read, L. K., & Vogel, R. M. (2016). Hazard function analysis for flood planning under nonstationarity. *Water Resources Research*, *52*, 4116–4131. https://doi.org/10.1002/2015WR018370

Reis, D. S. Jr., & Stedinger, J. R. (2005). Bayesian MCMC flood frequency analysis with historical information. *Journal of Hydrology*, *313*(1–2), 97–116. https://doi.org/10.1016/j.jhydrol.2005.02.028

Rigby, R. A., & Stasinopoulos, D. M. (2005). Generalized additive models for location, scale and shape. *Journal of the Royal Statistical Society: Series C: Applied Statistics*, *54*(3), 507–554. https://doi.org/10.1111/j.1467-9876.2005.00510.x

Salas, J. D. (1993). Analysis and modeling of hydrologic time series. In *Handbook of hydrology* (Chap. 19, pp. 1–72). New York: McGraw-Hill.

Sarhadi, A., Burn, D. H., Concepcion Ausin, M., & Wiper, M. P. (2016). Time-varying nonstationary multivariate risk analysis using a dynamic Bayesian copula. *Water Resources Research*, *52*, 2327–2349. https://doi.org/10.1002/2015WR018525

Schendel, T., & Thongwichian, R. (2017). Considering historical flood events in flood frequency analysis: Is it worth the effort? *Advances in Water Resources*, *105*, 144–153. https://doi.org/10.1016/j.advwatres.2017.05.002

Serinaldi, F., & Kilsby, C. G. (2015). Stationarity is undead: Uncertainty dominates the distribution of extremes. *Advances in Water Resources*, *77*, 17–36. https://doi.org/10.1016/j.advwatres.2014.12.013

Shi, F., Zhao, S., Guo, Z., Goosse, H., & Yin, Q. (2017). Multi-proxy reconstructions of May–September precipitation field in China over the past 500 years. *Climate of the Past*, *13*(12), 1919–1938. https://doi.org/10.5194/cp-13-1919-2017

Spiegelhalter, D. J., Best, N. G., Carlin, B. P., & Van Der Linde, A. (2002). Bayesian measures of model complexity and fit. *Journal of the Royal Statistical Society, Series B: Statistical Methodology*, *64*(4), 583–639. https://doi.org/10.1111/1467-9868.00353

Spiegelhalter, D. J., Best, N. G., Carlin, B. P., & Van Der Linde, A. (2014). The deviance information criterion: 12 years on. *Journal of the Royal Statistical Society, Series B: Statistical Methodology*, *76*(3), 485–493. https://doi.org/10.1111/rssb.12062

Stasinopoulos, D. M., & Rigby, R. A. (2007). Generalized additive models for location scale and shape (GAMLSS) in R. *Journal of Statistical Software*, *23*(7), 1–46. Retrieved from. https://www.jstatsoft.org/index.php/jss/article/view/v023i07/v23i07.pdf

Stedinger, J. R., & Cohn, T. A. (1986). Flood frequency analysis with historical and paleoflood information. *Water Resources Research*, *22*(5), 785–793. https://doi.org/10.1029/WR022i005p00785

Steinschneider, S., & Lall, U. (2015). A hierarchical Bayesian regional model for nonstationary precipitation extremes in Northern California conditioned on tropical moisture exports. *Water Resources Research*, *51*, 1472–1492. https://doi.org/10.1002/2014WR016664

Su, C., & Chen, X. (2019). Assessing the effects of reservoirs on extreme flows using nonstationary flood frequency models with the modified reservoir index as a covariate. *Advances in Water Resources*, *124*, 29–40. https://doi.org/10.1016/j.advwatres.2018.12.004

Sun, X., Lall, U., Merz, B., & Dung, N. V. (2015). Hierarchical Bayesian clustering for nonstationary flood frequency analysis: Application to trends of annual maximum flow in Germany. *Water Resources Research*, *51*, 6586–6601. https://doi.org/10.1002/2015WR017117

Swierczynski, T., Brauer, A., Lauterbach, S., Martín-Puertas, C., Dulski, P., von Grafenstein, U., & Rohr, C. (2012). A 1600 yr seasonally resolved record of decadal-scale flood variability from the Austrian Pre-Alps. *Geology*, *40*(11), 1047–1050. https://doi.org/10.1130/G33493.1

Toonen, W. H. (2015). Flood frequency analysis and discussion of non-stationarity of the Lower Rhine flooding regime (AD 1350–2011): Using discharge data, water level measurements, and historical records. *Journal of Hydrology*, *528*, 490–502. https://doi.org/10.1016/j.jhydrol.2015.06.014

Vallve, M. B., & Martin-Vide, J. (1998). Secular climatic oscillations as indicated by catastrophic floods in the Spanish Mediterranean coastal area (14th–19th centuries). *Climatic Change*, *38*(4), 473–491. https://doi.org/10.1023/A:1005343828552

Viglione, A., Merz, R., Salinas, J. L., & Blöschl, G. (2013). Flood frequency hydrology: 3. A Bayesian analysis. *Water Resources Research*, *49*, 675–692. https://doi.org/10.1029/2011WR010782

Villarini, G., Smith, J. A., Serinaldi, F., Bales, J., Bates, P. D., & Krajewski, W. F. (2009). Flood frequency analysis for nonstationary annual peak records in an urban drainage basin. *Advances in Water Resources*, *32*(8), 1255–1266. https://doi.org/10.1016/j.advwatres.2009.05.003

Vrugt, J. A., Ter Braak, C., Diks, C., Robinson, B. A., Hyman, J. M., & Higdon, D. (2009). Accelerating Markov chain Monte Carlo simulation by differential evolution with self-adaptive randomized subspace sampling. *International Journal of Nonlinear Sciences and Numerical Simulation*, *10*(3), 273–290. https://doi.org/10.1515/ijnsns.2009.10.3.273

Wang, Q. J. (1996). Using partial probability weighted moments to fit the extreme value distributions to censored samples. *Water Resources Research*, *32*(6), 1767–1771. https://doi.org/10.1029/96WR00352

Wang, W., Li, H. Y., Leung, L. R., Yigzaw, W., Zhao, J., Lu, H., et al. (2017). Nonlinear filtering effects of reservoirs on flood frequency curves at the regional scale. *Water Resources Research*, *53*, 8277–8292. https://doi.org/10.1002/2017WR020871

Xiong, B., Xiong, L., Xia, J., Xu, C. Y., Jiang, C., & Du, T. (2019). Assessing the impacts of reservoirs on downstream flood frequency by coupling the effect of scheduling-related multivariate rainfall with an indicator of reservoir effects. *Hydrology and Earth System Sciences*, *23*(11), 4453–4470. https://doi.org/10.5194/hess-23-4453-2019

Yan, L., Xiong, L., Liu, D., Hu, T., & Xu, C. Y. (2017). Frequency analysis of nonstationary annual maximum flood series using the time-varying two-component mixture distributions. *Hydrological Processes*, *31*(1), 69–89. https://doi.org/10.1002/hyp.10965

Yang, L., Li, J., Sun, H., Guo, Y., & Engel, B. A. (2019). Calculation of nonstationary flood return period considering historical extraordinary flood events. *Journal of Flood Risk Management*, *12*(2), e12463. https://doi.org/10.1111/jfr3.12463

Zhao, Y., & Zhu, J. (2015). Assessing quality of grid daily precipitation datasets in China in recent 50 years. *Plateau Meteorology*, *34*(1), 50–58 (in Chinese). http://www.gyqx.ac.cn/CN/10.7522/j.issn.1000-0534.2013.00141Retrieved from